Applied Catalysis B: Environmental 180 (2016) 687–697

Contents lists available at ScienceDirect

Applied Catalysis B: Environmental

journal homepage: www.elsevier.com/locate/apcatb

The preferential oxidation of CO in hydrogen rich streams over platinum doped nickel oxide catalysts

Ziyaad Mohamed, Venkata D.B.C. Dasireddy, Sooboo Singh, Holger B. Friedrich*

School of Chemistry and Physics, University of KwaZulu-Natal, Durban 4000, South Africa

ARTICLE INFO

Article history:
Received 18 March 2015
Received in revised form 8 June 2015
Accepted 8 July 2015
Available online 17 July 2015

Keywords:
Nickel oxide/alumina
Platinum/alumina
Preferential oxidation
Carbon monoxide and hydrogen

ABSTRACT

NiO/Al_2O_3, Pt/Al_2O_3 and $Pt/NiO/Al_2O_3$ catalysts were prepared by the incipient wetness technique with a Ni loading of 25 wt% and Pt loading of 0.5 wt%. These catalysts were characterized by ICP-OES, XRD, BET, TPR, N_2 adsorption–desorption isotherms, CO chemisorption, FTIR-CO, XPS, SEM-EDX and TEM. XRD and XPS results of the catalysts showed the presence of NiO and PtO phases on the respective supports and *in situ* redox reactions showed that the catalysts underwent reversible phase changes (oxide and metallic) that were stable. FTIR-CO studies showed that the Pt containing samples exhibited both linear and bridged CO adsorption with higher intensities observed for the $Pt/NiO/Al_2O_3$ catalyst. The catalysts were tested for the oxidation of CO in H_2 rich streams (preferential oxidation-PROX) in a continuous flow fixed bed stainless steel reactor. The NiO/Al_2O_3 catalyst produced very low conversions of CO in the stipulated PROX temperature range and showed highest conversion of 11% with a selectivity of 25% toward CO_2. The Pt/Al_2O_3 catalyst showed improved activity within the PROX temperature range with highest CO conversion of 56% and selectivity toward CO_2 of 68% at 200 °C. The $Pt/NiO/Al_2O_3$ catalyst revealed synergistic effects, obtaining much higher CO conversions within the PROX temperature ranges compared to both the mono-metallic catalysts. The highest CO conversion, of 99.9%, for this catalyst was at 200 °C, with a selectivity of 72.8% toward CO_2 using a $C:O_2$ ratio of 1:2.

© 2015 Elsevier B.V. All rights reserved.

1. Introduction

Hydrogen produced from fossil fuels has become a promising alternative to conventional fuel sources due to its low environmental impact, offering maximum power density as a fuel for proton exchange membrane fuel cell (PEMFC) applications [1–4]. One of the main concerns using hydrogen is safe storage for on-board applications, therefore on-board production following a series of catalytic reforming reactions, such as: steam reforming, autothermal reforming, partial oxidation and water-gas shift is more economically viable [5–7]. This reformate gas is supplied to the fuel cell stack for power generation [6]. However, following the water-gas shift reaction, trace amounts of CO (~1%) are still present in the feed stream [3,8–10]. This CO poisons a vital component of the PEMFC, which is the platinum electrode, leading to a loss in the fuel cell efficiency and hence its power output [6,9]. Preferential oxidation carried out after the conventional water-gas shift reaction provides a promising route for removing trace amounts of CO contaminants that may be present in the H_2 rich streams. This method is effective, offering ease of implementation, cost efficiency, reliability and safety for on-board fuel processing [10,11]. The reactions that take place in the preferential oxidation (PROX) reactor are shown below [12]:

$$CO + ½O_2 \rightarrow CO_2 \Delta H_{298K} = -283\,kJ/mol \quad (1)$$

$$H_2 + ½O_2 \rightarrow H_2O \Delta H_{298K} = -242\,kJ/mol \quad (2)$$

only the first reaction (Eq. (1)), the oxidation of CO to CO_2 is desired [12]. This reaction is usually accomplished at lower temperatures. The undesired H_2 oxidation reaction (Eq. (2)) is the key competitive reaction that takes place at higher temperatures and must be minimized to reduce the loss of H_2, while reducing CO concentrations to acceptable levels [2]. Thermodynamically, the enthalpy of H_2 reacting with O_2 is lower than that of CO reacting with O_2, however, with increasing temperature, H_2 prevents CO from adsorbing to some active sites of the catalyst [13]. PROX usually requires minimal amounts of surplus air corresponding to a CO/O_2 mole ratio or λ value of between 0.5 and 2 [12].

Early studies on PROX conducted by Oh and Sinkevitch [14] assessed the performance of a number of noble metals supported on alumina, and some transition metal based catalysts. Their results showed that among all the catalyst types tested, Pt, Ru and Rh were

* Corresponding author. Fax : +27 31 260 3091.
E-mail address: friedric@ukzn.ac.za (H.B. Friedrich).

http://dx.doi.org/10.1016/j.apcatb.2015.07.012
0926-3373/© 2015 Elsevier B.V. All rights reserved.

the most efficient catalysts with regards to selectivity toward CO_2. Following this work, many catalytic formulations have been tested for the PROX reaction and among all the metals, Au, Rh, Ru, Pt, Ir and Pd supported on Al_2O_3, MgO, CeO_2, ZnO, TiO_2 and SiO_2 showed good activity within the desired temperature ranges [3,15–18]. However, when using precious metal catalysts for the PROX reaction, high costs and limited durability are of main concern, therefore, research at present is directed toward alternative, more cost effective catalysts that show similar activity toward the PROX reaction [19]. These could make use of cheaper metals and also include a low content of noble metal, instead of using them as the bulk catalyst.

Several Pt catalytic system have already been investigated for the PROX reaction and Pt catalysts are also known to function well in fuel processors, working at high temperatures, and they are resistant toward catalyst deactivation [4,11]. Many efforts have also been made at improving the selectivity and activity of Pt catalysts by adding an additional metal. These minimize the adsorption of CO which tends to block the adsorption sites of O_2 on the Pt, making CO oxidation more difficult.

Ko *et al.* [20] reported that mono-metallic Pt catalysts usually exhibit noticeable PROX activity above 150 °C. Their findings also indicated that PROX activity at lower temperatures could be enhanced by the addition of a second metal such as Fe, Co, Ni, Mn or alkali metals. These authors found that the addition of Ni to the catalyst was more effective over a wide temperature range and showed higher CO conversion and selectivity toward CO_2.

These results motivated our study in utilising a low Pt content, instead of using it as a bulk catalyst, toward developing a relatively inexpensive catalyst containing Ni which is used in one or more of the on-board reforming steps (steam reforming and partial oxidation) [21,22]. In this study a 25 wt% NiO/Al_2O_3 catalyst was synthesized, characterized and tested for PROX activity within the stipulated temperature ranges. To this catalyst 0.5 wt% Pt was added and the material characterized and tested.

2. Experimental

2.1. Catalyst synthesis

The γ-aluminum oxide (Al_2O_3) support was purchased from Alfa Aesar, Karlsruhe, Germany. The NiO/Al_2O_3 (25 wt%) denoted as Ni–Al, Pt/Al_2O_3 (0.5 wt%) denoted as Pt–Al and the $Pt/NiO/Al_2O_3$ denoted as Pt–Ni–Al catalysts were prepared by the incipient wetness technique adopted from literature [23]. For the Ni–Al catalysts, $Ni(NO_3)_2.6H_2O$ (Sigma–Aldrich, 98%) was dissolved in a minimum amount of deionized water and added to a slurry of γ-Al_2O_3 and deionized water, with vigorous stirring at room temperature for an hour. Water was evaporated on a hot plate at 80 °C until a paste was obtained. The paste was oven dried overnight at 110 °C, thereafter calcined at 500 °C. For the Pt–Al catalyst, $H_2PtCl_6.6H_2O$ (BDH Chemicals, 40%) was used for the synthesis (as described for the Ni–Al catalyst) and calcined at 300 °C. The Pt–Ni–Al catalyst was prepared by adding $H_2PtCl_6.6H_2O$ dissolved in a minimum amount of deionized water to a slurry of deionised water and the Ni–Al catalyst and calcined at 300 °C.

2.2. Catalyst characterization

2.2.1. Inductively coupled plasma-optical emission spectroscopy

The elemental composition of the fresh catalysts was determined using an Optima 5300 DV PerkinElmer Optical Emission Spectrometer. Accurately weighed catalyst samples (0.50 g), were dissolved in 5 mL HNO_3 and digested using a PerkinElmer Multiwave microwave sample preparation system operating at 600 W. Standards solutions for Ni and Pt (Industrial Analytical, RSA) were prepared ranging from 0 to 100 ppm.

2.2.2. Physisorption-N_2 adsorption–desorption and pore size distribution (PSD)

The fresh and used catalyst samples (~0.2 g) were degassed under a steady stream of nitrogen using a Micromeritics Flow Prep 060 Sample degas system. A temperature ramp of 2 °C per min was applied until a final temperature of 200 °C was reached and the samples were kept constant at this temperature overnight. Thereafter, samples were analysed using a Micromeritics TriStar II Surface Area Analyser. The same instrument was used to determine the pore size distributions using the method of Barret, Joyner and Halenda (BJH).

2.2.3. Powder and in situ X-ray diffraction

Powder X-ray diffraction (XRD) patterns of the fresh and used catalysts were recorded on a Bruker D8 Advance instrument with Diffracplus XRD Commander Software and a Bruker VANTEC detector. The radiation source used was Cu Kα (wavelength of 0.1540 nm), operating on a long focus line with a voltage and amperage of 40 kV and 40 mA respectively. The catalysts were scanned in a 2θ range from 2° to 90° at 0.5° per minute. For *in situ* redox experiments, 5% H_2 in nitrogen was used as the reducing gas and air as the oxidizing gas. The temperature was ramped from room temperature to 600 °C at 50 °C increments and gradually cooled to 100 °C.

2.2.4. Temperature programmed techniques

Temperature programmed reduction (TPR) profiles were obtained using a Micromeritics Autochem II Chemisorption Analyzer. Approximately 0.05 g of the fresh calcined catalyst sample was placed in a U shaped quartz tube. Prior to reduction, the catalysts were pre-treated by heating to 400 °C under a stream of argon (30 mL/min) for 30 min and the temperature was decreased to 90 °C under the same stream of argon. The reduction experiments were carried out using 5 vol.% H_2 in Ar as the reducing agent with a flow rate of 30 mL/min to a temperature of 1000 °C ramped at 10 °C/min.

2.2.5. CO Chemisorption

Fresh catalyst samples (~0.15 g) were degassed under a flow of N_2 from room temperature to 200 °C and then kept under vacuum for 12 h using a Micromeritics Flow Prep 060 Sample Degas System. Samples were analysed using a Micromeritics ASAP 2020 instrument. Samples loaded in a quartz tube were initially reduced with H_2 at 700 °C for 2 h. The chemisorption of CO on the materials was analysed at 35 °C within a pressure range of 200–400 mmHg. The metal dispersions and crystallite sizes were calculated from the CO adsorption data using a stoichiometric ratio of 1.

2.2.6. FTIR CO

FTIR-CO measurements were recorded using a Bruker Tensor 27 with Harrick DRIFTS accessory and Harrick high temperature reaction chamber. The catalyst samples were compressed into self-supporting wafers (~20 mg/cm^2) and mounted in the IR cell which allowed both heating (200 °C) and cooling (RT) *in situ* under atmospheric pressures. The fresh catalyst samples were degassed under Ar (30 mL/min) at 200 °C for 6 h prior to each experiment. CO gas was pulsed through a VICI loop size of 100 μL over the samples at 35 °C and 200 °C and flushed out with Ar between each pulse.

2.2.7. X-ray photon spectroscopy (XPS)

A Kratos Axis Ultra DLD spectrometer, fitted with an achromatic Al K source operated at 120W was used for XPS analysis. During the analysis, the pressure in the chamber was maintained around 1×10^{-9} mbar. The acquisition of survey and detailed regional scans

were obtained using pass energies of 160 eV and 40 eV, respectively. Binding energy calibrations were done against the standard C 1 s signal from adventitious carbon contamination (assumed to be a binding energy of 284.7 eV) [24].

2.2.8. Microscopic analyses

Scanning electron microscopy (SEM) images were obtained using a FEG 1450 Scanning Electron Microscope at 20 kV. Energy dispersion X-ray (EDX) was carried out using a Jeol JSM 6100 Scanning Electron Microscope equipped with a Bruker EDX Detector and analysed with Espirit 1.8.5 software. Samples for EDX were coated with carbon in a Jeol JEE-4C Vacuum Evaporator, whereas fresh samples for SEM images were coated with gold using a Polaron SC Sputter Coater. For transmission electron microscopiy (TEM), fresh catalyst samples were diluted with ethanol in an Eppendorf tube and sonicated for 2 min. Samples were then coated on a formvar copper grid and were viewed using a Jeol JEM 1010 TEM instrument operated at a voltage of 100 kV. Images were captured with a MegaView III Soft Imaging System. TEM measurements were done using iTEM software on the instrument and exported.

2.3. Catalytic testing

All gas phase oxidation reactions were carried out in a continuous flow fixed bed reactor. The reactor tube was made of ¾ inch (outer diameter) stainless tubing, 49 cm in length. The catalyst bed consisted of 0.75 mL catalyst (pellet sizes between 300 and 600 μm) diluted in 2.25 mL 24-grit carborundum and was always located at the isothermal point within the reactor tube. All void spaces in the reactor tube were filled with 24-grit carborundum. A coaxially centered thermocouple was used to monitor the temperature of the catalyst bed and the reactor furnace. The thermocouples were controlled by CB-100 RK temperature control units. The gaseous mixture was introduced into the reactor system using Brooks mass flow controllers (MFCs). A simulated reformate feed containing 1 vol.% CO, 0.5–2 vol.% O_2, 50 vol.% H_2 balanced with N_2 (48.5 vol.%) was used for catalyst testing. The flow rate was set at 150 mL/min and the GHSV fixed at 12,000 h^{-1}. The catalysts were tested at temperatures ranging from room temperature to 200 °C. For total CO oxidation reactions hydrogen was excluded from the reaction mixture. To maintain the flow rate at 150 mL/min, the concentration of N_2 was adjusted. For these reactions, the temperatures tested ranged from room temperature to 250 °C for Pt containing samples and 300 °C for the mono-metallic Ni sample. The gaseous products were analyzed using an on-line, 3 channel Varian CP-4900 Micro GC equipped with a thermal conductivity detector (TCD). Carbon and oxygen balances calculated were between 98 and 102% and all data points were obtained in triplicate with an error of ±1%. The selectivity toward CO_2 is calculated as the mol% formed from the total products ($CO_2 + H_2O$).

3. Results and discussion

3.1. Catalyst characterization

3.1.1. Inductively coupled plasma-optical emission spectroscopy

The metal content of the catalysts were quantitatively determined by inductively coupled plasma-optical emission spectroscopy (ICP-OES). The weight percentages of the metals obtained were similar to the nominal weight loadings (Table 1). However, with the Pt–Ni–Al catalyst a slightly lower percentage of Ni was obtained. This could be due to some displacement of the Ni during the synthesis with an acidic Pt precursor.

Table 1
Elemental composition of the catalysts.

Catalyst	Nominal weight (%)		Weight (%) (From ICP)	
	Pt	Ni	Pt	NI
Ni–Al	–	25	–	24.6
Pt–Al	0.5	–	0.45	–
Pt–Ni–Al	0.5	25	0.56	21

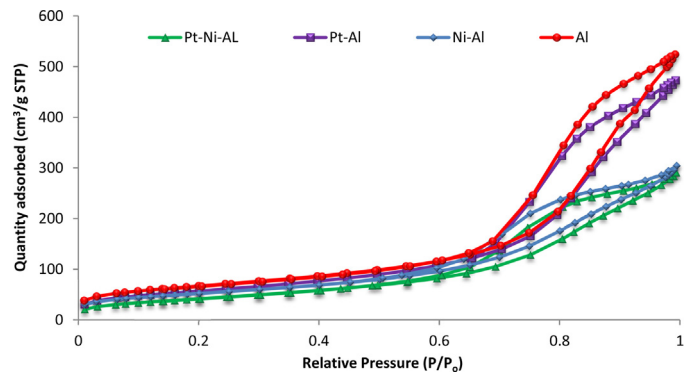

Fig. 1. N_2 adsorption–desorption isotherms of catalysts.

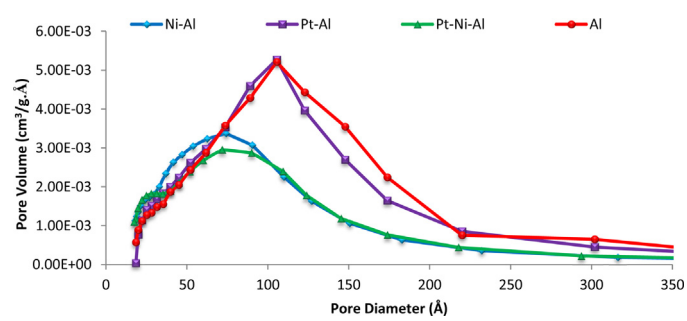

Fig. 2. Pore size distributions (PSDs) of the catalysts.

3.1.2. Physisorption analyses-N_2 adsorption–desorption

N_2 adsorption–desorption isotherms of the support and catalysts are shown in Fig. 1. All samples show typical type IV isotherms in the classification of Brunauer, Deming, Deming and Teller (BDDT) [25], with H1 hysteresis loops which are characteristic for mesoporous materials [26]. The steepness of the capillary condensation steps clearly indicates uniformity of the mesopores. Following the impregnation of Ni (25%) on Al_2O_3, there is a significant decrease in the steepness of the capillary condensation step which correlates closely to data reported in the literature, as the amount of metal increases on the support the volume capacities of N_2 adsorbed decreases [25,26]. With regards to the Pt containing samples, due to the low amount of Pt (0.5%) there is a slight decrease in the quantity of N_2 adsorbed. Fig. 2 shows the corresponding pore size distributions (PSDs) of the samples within the mesoporous region. All samples studied show the absence of macropores and exhibit a flat baseline upwards from 220 Å. It is clearly visible for materials containing Ni (Ni–Al and Pt–Ni–Al), from the steepness of the capillary condensation steps that represent broader isotherms across the relative pressure (P/P_o), that the corresponding PSDs generated have a broader pore size range. For the mono-metallic Pt–Al material, the adsorption isotherm has a narrower condensation step, representing narrow distributions for the corresponding PSD curves generated, which is also evident in the literature [26].

After the impregnation of Pt onto the support, as well as onto the mono-metallic Ni–Al catalyst, the surface areas and the pore volumes decrease compared to those of the Al_2O_3 support and the

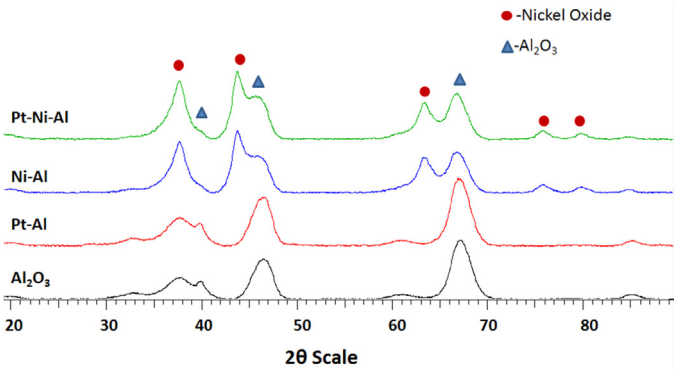

Fig. 3. Powder X-ray diffractograms of the catalysts.

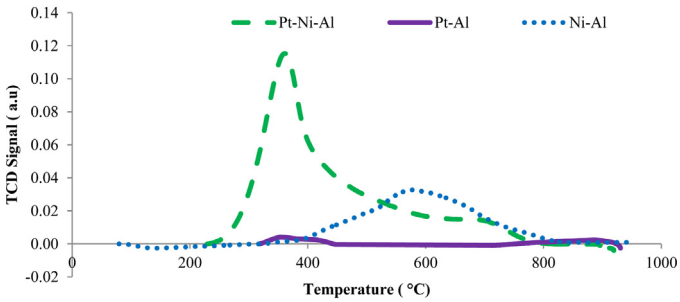

Fig. 4. TPR profiles of the supported catalysts.

mono metallic Ni–Al catalyst. Pore diameters, however, tend to show a slight increase, which may be due to the additive effect of Pt by the impregnation method. According to Li *et al.* an increase in the pore diameter is most likely due to the tendency of the Pt atoms to be preferably located on the surface of the support, resulting in the possible formation of Pt–Ni alloys.

3.1.3. Powder X-ray diffraction

Fig. 3 shows the stacked X-ray diffractograms of the samples. The characteristic peaks for γ-Al_2O_3 are observed at 2θ values of 37.18°, 39.3° 45.36° and 66.71° corresponding with d spacing values of 2.39, 2.28, 1.97 and 1.52. These d spacings correspond to those listed in the JCPDS File No: 10-425. Characteristic peaks at 2θ values of 37.18°, 43.26°, 45.36°, 62.5° and 66.71° with d spacings of 2.41, 2.08, 1.99, 1.48 and 1.40, respectively, clearly indicate the presence of NiO particles (JCPDS File No: 4-0835 and ICDD files obtained using Peak Match Software). Pt characteristic peaks could not be detected at these low wt% loadings.

3.1.4. Temperature programmed reduction

The TPR profiles of the catalysts are shown in Fig. 4. The Ni–Al catalysts show a slight negative peak in the temperature region of 100-200 °C which is attributed to physisorbed moisture on the surface of the catalysts. The onset reduction temperature for the Ni–Al catalysts is within the temperature region of 300–400 °C. According to Ren *et al.* [27], these high temperature reductions for high NiO loadings can be attributed to the reduction of Ni^{2+} ions incorporated into tetrahedral and octahedral vacancies on the surface of the Al_2O_3 support. The increase in the broadness and peak shoulder at 670 °C could be an indication that NiO particles are loosely bound to the support, and these particles saturate the surface of the support forming bulk NiO [28]. For the mono-metallic Pt–Al catalyst, a broad reduction peak is observed at around 350 °C, which can be assigned to the reduction of platinum oxide to its metallic form [29]. There is a pronounced influence on the NiO reduction temperature for the Pt–Ni–Al sample following the addition of Pt. The reduction temperature shifts to a lower temperature, attributed mainly to the change in mechanism of the NiO reduction [21,29,30].

De Souza *et al.* [21] reported that the reduction of Pt oxide takes place before reduction of the Ni oxides. The resulting Pt^0 sites formed are available to activate H_2 to atomic $H^\bullet$ at much lower temperatures compared to those required for H_2 activation on NiO. The surface of the NiO then receives this transferred $H^\bullet$ through a spillover mechanism, reducing the NiO to Ni^0 at a lower temperature. This mechanism suggests that the nucleation of the Ni^0 is controlled by the activation of H_2. The shoulder peak observed in the TPR of Pt–Ni–Al at higher temperatures is attributed to the NiO species that are still interacting strongly with the support [21,28]. From Table 3, it can be seen that the hydrogen consumption and degree of reducibility is higher for the Pt–Ni–Al catalyst compared to the mono-metallic Pt–Al catalyst. Also, this higher consumption of H_2 is attributed to the presence of the NiO, also present in the Pt–Ni–Al catalyst, which now reduces at lower temperatures, due to the strong metal–metal oxide interactions between the Pt and Ni particles on the surface of the support [31].

3.1.5. *In situ* XRD

From Fig. 5(A), Ni–Al under a reducing atmosphere shows no phase change for the NiO until 450 °C, corresponding to the results obtained from the TPR. Also no observable change is seen regarding to the crystallinity of the catalyst within the temperature range of 100–400 °C, indicating that the catalyst is stable up to 400 °C under the reducing environment. The scheme in Fig. 6(A) shows phases of NiO, Ni_2O and Ni metal that are observed within the temperature range 450–600 °C, which indicates the reduction pathway of NiO. These phases are confirmed with the ICDD File Nos: 10,870,712 (Ni), 10,721,464 (Ni_2O) and 10,780,429 (NiO) with peaks at 2θ values of 44.53°, 51.83°, 62.79° and 76.73°, corresponding to d spacings of 2.03, 1.76, 1.47 and 1.24 respectively. The complete reduction of NiO to Ni occurs at 600 °C. Ni remained in its metallic form when the catalyst was gradually cooled to 100 °C. The oxidation of the Ni metal to the NiO phase takes place within the temperature range of 100–300 °C, following the inverse pathway to the reduction, which is shown in Fig. 6(A). This transformation of the Ni metal to the NiO phase via the intermediate Ni_2O phase is evident and confirmed by the following ICDD file Nos: 10,870,712 (Ni), 10,721,464 (Ni_2O) and 10,780,429 (NiO). The characteristic peaks of Ni, NiO and its intermediate Ni_2O phase are now seen within the temperature region of 100–300 °C. The complete oxidation of Ni metal to NiO occurs at about 400 °C and the Ni remained in its oxide form when the catalyst was cooled to 100 °C. This *in situ* reduction and re-oxidation (Fig. 5A) indicates that the catalyst is stable under redox conditions and has reversible phase changes.

Table 2
Particulate properties of the fresh catalysts.

Catalyst	Surface area (m^2/g)	Pore volume (cm^3/g)	Pore diameter (Å)	Metal Dispersion (%)	Crystallite Size (nm)
Alumina	225	0.78	127.6	–	–
Ni–Al	189	0.47	94	19	5
Pt–Al	207	0.70	128.1	39	3
Pt–Ni–Al	156	0.43	110.3	14	7

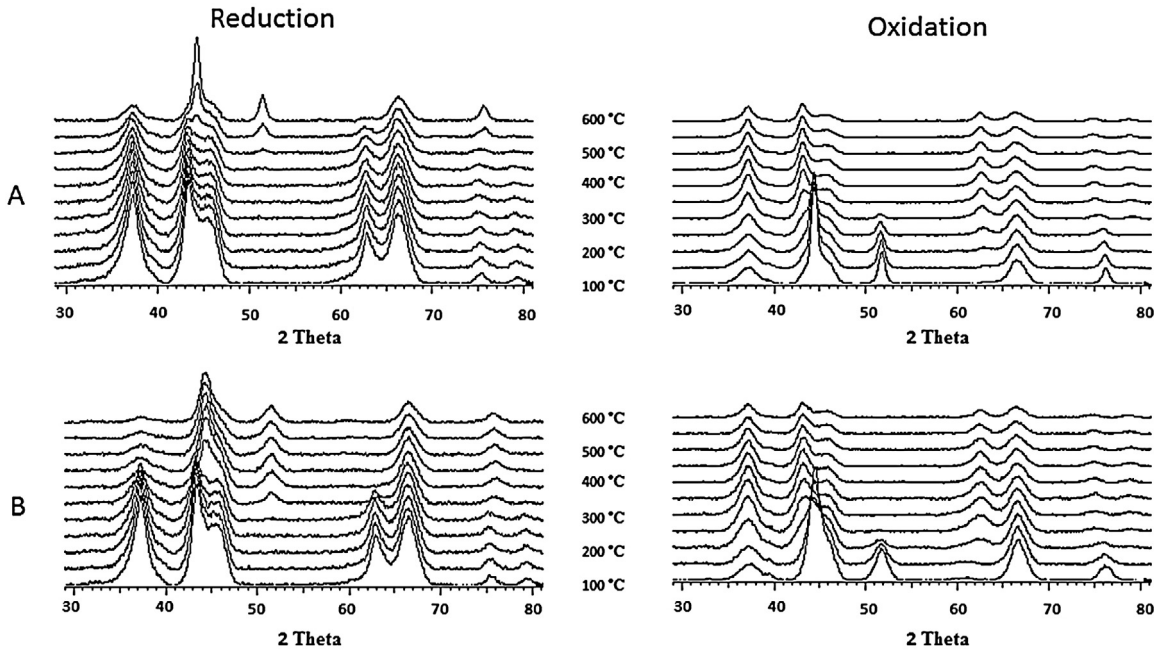

Fig. 5. In-situ X-ray diffractograms of (A) Ni–Al and (B) Pt–Ni–Al.

Fig. 5(B) shows the *in situ* XRD traces for Pt–Ni–Al under a reducing atmosphere, where no observable change is seen in the crystallinity of the catalyst within the temperature region of 100–300 °C, indicating that the catalyst is stable up to 300 °C. However, compared to the mono-metallic Ni–Al catalyst, reduction starts from ±350 °C, suggesting that the impregnation of Pt promotes NiO reduction, which was evident from the TPR profiles obtained. The phases of NiO, Ni_2O and Ni metal are observed within the temperature region 350–600 °C, showing a reduction pathway of NiO similar to that of the mono-metallic Ni–Al catalyst. The complete reduction of NiO to Ni occurs at a temperature of 550 °C and the Ni remained in its metallic form when the catalyst was cooled to 100 °C. The presence of the Pt phases on the Pt–Ni–Al catalyst cannot be seen due to the low loading of Pt. According to Li *et al.* [30], Pt binds to the Ni particles present on the support and forms alloys and therefore will not be clearly identified by XRD.

The transformation of the Ni metal to the NiO phase in air takes place within the temperature range of 100–250 °C, suggesting that the impregnation of Pt on the Ni–Al catalyst also promotes its oxidation. The transformation also follows the inverse pathway to the reduction of NiO shown in Fig. 6(B). Characteristic peaks of Ni, NiO and its intermediate Ni_2O phases are now seen within the temperature range of 100–200 °C. The complete oxidation of Ni metal to NiO occurs at about 250 °C and the Ni remained in its oxide form when the catalyst was cooled to 100 °C. Thus, from *in situ* XRD experiments, the Pt–Ni–Al catalyst is reduced to its metallic form, which is then re-oxidized to its oxide phase at lower temperatures compared to the Ni–Al catalyst. Furthermore, this catalyst is stable under redox conditions and undergoes reversible phase changes.

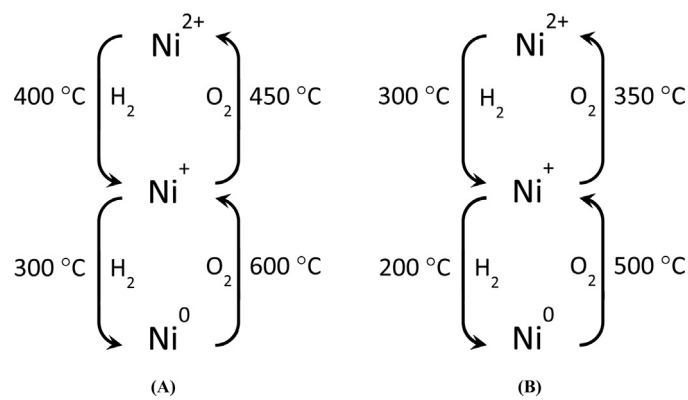

Fig. 6. Reduction-oxidation of nickel in (A) Ni–Al and (B) Pt–Ni–Al catalysts.

3.1.6. CO Chemisorption

The metal dispersions determined for the supported catalysts are shown in Table 2. There is an average Ni dispersion of 19% on the Ni–Al catalyst, with an average crystallite size of 5 nm. The Pt–Al catalyst has a higher metal dispersion of 39% with a smaller average crystallite size of 3 nm compared to both the Ni containing samples. These Pt particles are well dispersed compared to the Pt–Ni–Al catalyst, which showed a metal dispersion of 14% with an average crystallite size of 7 nm. The lower dispersion and larger crystallite size of the Pt–Ni–Al catalyst is probably due to the Pt atoms alloying with the Ni particles present on the support following the impregnation [30]. If Pt had interacted with the surface of the support of the mono-metallic Ni–Al catalyst, it would show an increase in the metal dispersion. This also correlates to the results obtained from the surface characterization data (Table 2) which shows that after the impregnation of Pt on the Ni–Al catalyst the pore volume decreases whilst the pore diameter for the catalyst increases slightly.

Table 3
TPR data obtained for the fresh catalysts.

Catalyst	Temperature (°C)	H_2 consumption (cm^3/g)	Degree of reducibility (%)
Ni–Al	624	65.3	69.1
Pt–Al	330	6.0	3.9
Pt–Ni–Al	330	64.1	71.0
	587	19.0	13.0

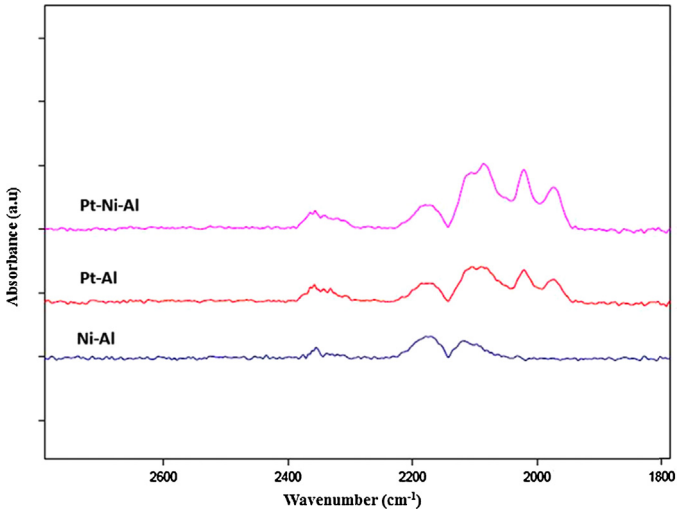

Fig. 7. FTIR-CO of the prepared catalyst samples at 200 °C.

3.1.7. FTIR-CO

Fig. 7 shows the DRIFTS FTIR-CO of the samples analyzed at 200 °C. The DRIFTS CO spectrum of Ni–Al showed bands at 2030, 2024, 2134 and 2192 cm^{-1}. According to Dalmon *et al.* [32], the bands observed in the higher frequency region of 2100–1950 cm^{-1} can be related to CO species linearly bonded to one Ni atom (Ni–CO). Bands in the lower-frequency region of 1900–1750 cm^{-1}, are related to CO bonded on two or more surface metal atoms (bridged-bonded (Ni_x–CO, $x > 1$)), respectively. Since there is no bridging CO band observed in the spectrum of the Ni–Al catalyst, this could indicate that NiO is well dispersed on the surface of alumina [33]. For the Pt–Al catalyst, the bands are observed at 1992, 2048, 2080, 2110 and 2173 cm^{-1}. Bands observed at 2080 and 2110 cm^{-1} are due to the linearly adsorbed CO on Pt [34], whereas bands at 1992 and 2048 cm^{-1} could be for bridge-bonded CO on two Pt atoms and/or CO adsorbed on the interface between the Pt and the surface of the support [35]. For the Pt–Ni–Al catalyst, the CO bands are observed at 1975, 2021, 2080, 2107 and 2173 cm^{-1}. Since both Pt and Ni have similar carbonyl bands, it is difficult to specifically allocate the bands to the metals in the Pt–Ni–Al catalyst. There is no shift in the bands around 2080 and 2173 cm^{-1} which represent the linearly adsorbed CO on the Pt metal of the catalyst [34]. Also, the positions of the bands of CO adsorbed on Pt and Ni in the low frequency regions are similar, making them difficult to distinguish. However, the intensity of these bands is higher for the Pt–Ni–Al catalyst compared to the mono-metallic catalysts. There is a slight shift in the band at around 2100–2200 cm^{-1} when comparing Ni–Al to the Pt–Ni–Al. This could be associated with a change of the electronic state of the metal atoms under CO, which could also be related to the degree of reducibility for the Pt–Ni–Al catalyst (Table 3) [33].

3.1.8. X-ray photon spectroscopy

XPS was used to show the presence of the active metals on the surface of the supports, as well as the oxidation states. Table 5 lists the binding energies corresponding to Ni $2p_{3/2}$, Ni $2p_{1/2}$, Pt $4f_{7/2}$, Pt $4f_{5/2}$ and O 1s levels for all the prepared samples and Fig. 8 shows the Ni 2p, Pt 4f and O 1s spectra obtained for the Pt–Ni–Al catalyst. The data for the Ni on the surface of the catalyst is characteristic for Ni^{2+} ions as shown by the $2p_{3/2}$ transitions, with peaks present at eV = 853 and 859 [25]. Also the presence of two satellites due to NiO is shown by the $2p_{1/2}$ transitions at eV = 871, and 877 along with the split spin-orbit components (Δ = 18 eV) [36,37]. The positions of the Pt 4f peaks appear as the sum of two broad peaks characteristic for Pt^{2+} at eV = 72.7 and 76.0 corresponding to levels $4f_{7/2}$ and $4f_{5/2}$ [18,38,39]. The O 1s spectrum for all the catalysts showed a standard peak at eV = 529.4 which is characteristic for Ni–O and Pt–O [38–40]. Additionally, the wt% obtained from XPS is similar to the ICP results.

Table 4
Particulate properties of the used catalysts.

Catalyst	Surface area (m^2/g)	Pore volume (cm^3/g)	Pore diameter (Å)
Ni–Al	164	0.42	108
Pt–Al	163	0.30	90
Pt–Ni–Al	95	0.25	109

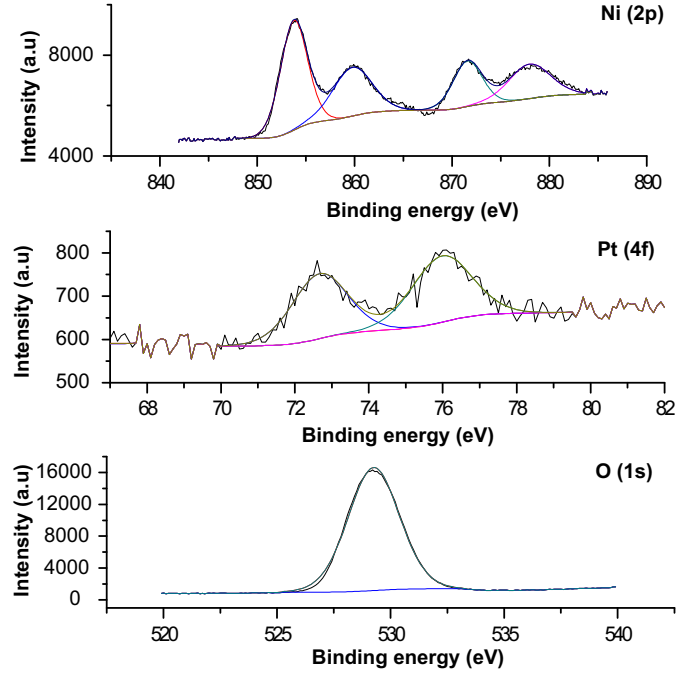

Fig. 8. XPS spectra of the Pt–Ni–Al catalyst.

3.1.9. Microscopic analyses

SEM images (Supplementary information, Fig. S1) show the surface morphology of the catalysts. Al_2O_3 particles (Supplementary information, Fig. S1A) tend to form globules which comprise of many primary particles with their dimensions being only a few micrometers [41]. Following the impregnation of NiO on the support (Supplementary information, Fig. S1B), the surface of the support becomes a little rougher and the particles are irregular and wrinkled. Kiss *et al.* [41] stated that for impregnated NiO/Al_2O_3 catalysts, the presence of the Al_2O_3 phase becomes invisible due to the NiO phase forming shell-like coverings of various thickness around the Al_2O_3 particles. This "shell" catalyst can ensure maximum use of the active component and gives greater thermal stability of the catalyst [41]. After the impregnation of Pt on the support (Supplementary information, Fig. S1C) and on the mono-metallic Ni–Al catalyst (Supplementary information, Fig. S1B), no change in the surface morphology is observed due to the higher amounts of NiO present compared to Pt. The SEM-EDX mappings of all the catalysts show an even distribution of the active metal particles on the support and the presence of the metals (Supplementary information, Figs. S2–S5). This data correlates with results obtained from ICP, chemisorption and XRD data.

Fig. 9 shows the TEM images of the catalyst samples. From the images (Fig. 9A and B), the interface between the nickel particles (dark spots) and alumina support is not well defined. However, the dispersion of nickel across the support was uniform. The mor-

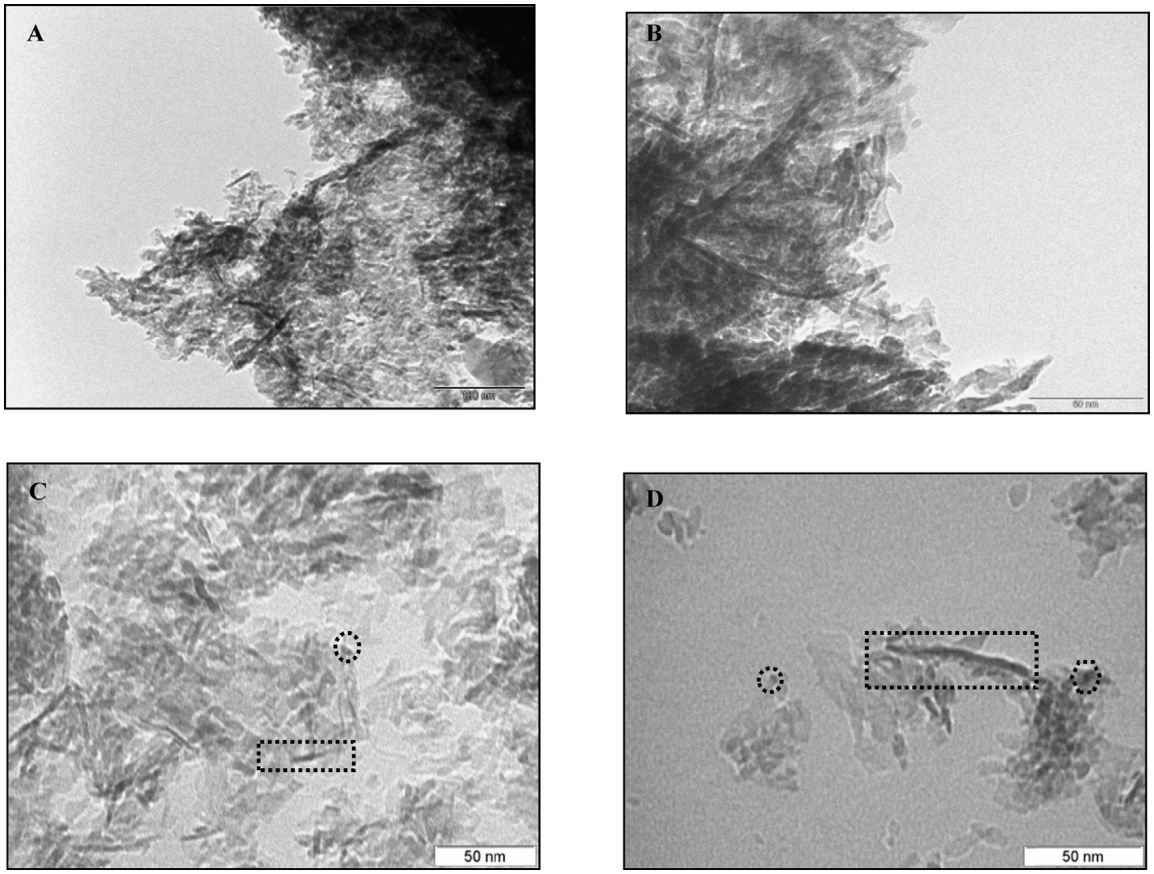

Fig. 9. Transmission electron micrographs of (A) the Al_2O_3 support, (B) Ni–Al (C) Pt–Al and (D) Pt–Ni–Al.

phology of the particles is spherical and rod-shaped with minimum aggregation, relating closely to data obtained by Ghule *et al.* [42]. For the Ni–Al catalyst (Fig. 9B), the NiO particles are more distinctly pronounced and visible, due to the catalyst being more crystalline [42]. For the Pt–Al (Fig. 9C) and Pt–Ni–Al (Fig. 9D) catalysts, the Pt particles are uniformly distributed across the surface of the supports, (denoted by a circle) and agrees with micrographs presented by Liu *et al.* [43]. For the Pt–Ni–Al (Fig. 9D), the presence of larger particles is attributed to the Ni species also present on the support (denoted by a rectangle). The measured Ni particle sizes were in the range of 5–12 nm, whereas the Pt particle sizes ranged from 2 to 3 nm (Supplementary information, Figs. S6–S8). These results correlate closely with the crystallite sizes calculated from CO chemisorption experiments.

3.2. Catalytic testing

Initially, two blank reactor studies (24-grit carborundum and γ-Al_2O_3) were carried out. These blank reactions showed no conversion of CO in all experiments.

3.2.1. Total CO oxidation

Using a flow rate of 150 mL/min and a GHSV of 12,000 h^{-1}, the prepared mono-metallic catalysts were tested for CO oxidation reactions with varying C:O_2 ratios (1:0.5, 1:1 and 1:2).

The mono-metallic Ni–Al catalyst was tested from room temperature to 290 °C. This is beyond the desired PROX temperature range, but according to Wang and Lu [44] NiO supported materials are more active for oxidation reactions at higher temperatures. The onset temperature for the oxidation of CO over the Ni–Al catalyst at the studied C:O_2 ratios is 150 °C. An increase in the activity for these catalysts is observed at temperatures close to 300 °C. Increasing the O_2 concentration improves CO conversion (Fig. 10A), resulting in lower O_2 conversions (Fig. 10B). A maximum conversion of 48% was obtained for this catalyst at 290 °C employing a C:O_2 ratio of 1:2.

The mono-metallic Pt–Al catalysts were tested from room temperature to 250 °C. Results show similar trends to the mono-metallic Ni–Al catalyst where increases in both temperature and O_2 concentrations improve CO conversion. Almost complete oxidation of CO for this catalyst was obtained at 220 °C, and this remains constant up to 250 °C employing a C:O_2 molar ratio of 1:2.

3.2.2. Preferential oxidation

3.2.2.1. Time on stream. The activities of the catalysts were investigated under PROX conditions over 24 h using a C:O_2 ratio of 1:0.5 at 150 °C with a flow rate of 150 mL/min and a space velocity of 12,000 h^{-1}. CO conversions and selectivity toward CO_2 were stable for the full duration of the experiments.

3.2.2.2. Activity measurements for PROX reactions. The catalysts were tested for PROX activity from room temperature to 200 °C. Also, from the trends observed for the CO oxidation reactions, only C:O_2 ratios of 1:0.5 and 1:2 were investigated. The results obtained for the mono-metallic and the bi-metallic catalysts are shown in Fig. 11.All show very low CO conversions below 100 °C. These results can be correlated to the FTIR-CO, where at 35 °C, no CO adsorbs onto the catalysts (Supplementary information, Fig. S9). However, at 200 °C, the presence of CO bands in the FTIR spectra of all the catalyst samples implies significant adsorption (Fig. 7). The mono-metallic Ni–Al catalyst shows very low CO conversions beyond 100 °C, reaching a maximum of 3% at 200 °C (Fig 11A).

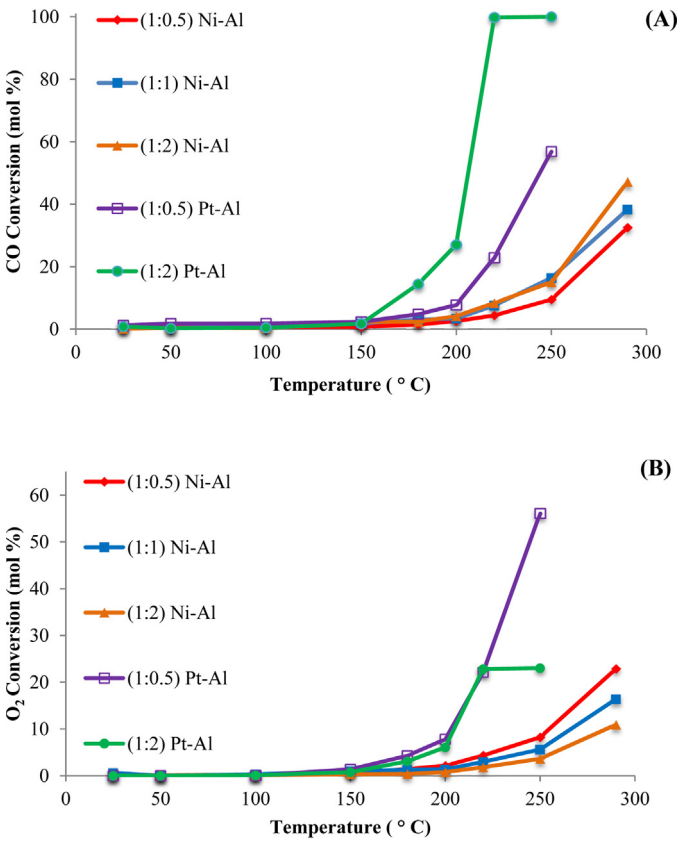

Fig. 10. CO (A) and O_2 (B) conversions for the CO oxidation reactions over the catalysts employing C:O_2 of 1:0.5, 1:1 and 1:2 using a GHSV of 12,000 h^{-1}.

This catalyst was tested beyond 200 °C and the results showed that the catalyst was more active at higher temperatures, unfortunately beyond the useful PROX temperature range. Selectivity of this catalyst to H_2O (Fig. 11E) is higher at lower temperatures and decreases as the temperature increases compared to the CO_2 selectivity (Fig. 11D). O_2 conversion (Fig. 11B) for this catalyst was relatively low.

The mono-metallic Pt–Al catalyst shows better activity in the preferential oxidation of CO from 100 °C onwards for both C:O_2 ratios. As temperature increases, CO conversion (Fig. 11A), O_2 conversion (Fig. 11B) and selectivity toward CO_2 (Fig. 10.D) also increases. The selectivity toward CO_2 increases from 10% to 55% at 150 °C and it reaches 69% at 200 °C when employing a C:O_2 ratio of 1:2. The selectivity toward H_2O (Fig. 11E) decreased with temperature and was at its lowest when the CO conversion was at its highest. The O_2 conversion at maximum CO conversion, employing a C:O_2 ratio of 1:2, was only 20%, confirming that increasing the O_2 content in the feed increases CO conversion and decreases the O_2 conversion. Of the two mono-metallic catalysts tested, the Pt catalyst is clearly much more effective for the oxidation of CO in H_2 rich streams. This is also evident from the FTIR-CO adsorption capacity of the materials, since Pt–Al showed more CO bonding compared to the Ni–Al catalyst.

Pt–Ni–Al, on the other hand, exhibits a similar trend to the Pt–Al catalyst, showing activity from 100 °C onwards (Fig 11A). These results can be related to the FTIR-CO of this catalyst which was almost similar to that of the Pt–Al catalyst. However, in comparison to the mono-metallic catalysts, this catalyst shows a synergistic effect with regards to the activity toward the oxidation of CO in the presence of H_2 with both the C:O_2 ratios screened. This is also supported by the higher intensity of the bands in the FTIR-CO compared to the Pt–Al and Ni–Al catalysts. Using a C:O_2 ratio of 1:0.5 a maximum CO conversion of 60.9% is obtained at 200 °C with a selectivity toward CO_2 of 75.4%. Using a C:O_2 ratio of 1:2 for this catalyst a CO conversion of 97% is obtained at 180 °C and reaches a maximum at 200 °C. The selectivity toward CO_2 reaches a maximum of ±74% at 180 °C and decreases slightly to ±73% at 200 °C (Fig 11D). This is due to the oxidation of H_2 that starts taking place [45]. Two competitive reactions are taken into consideration: firstly the CO oxidation (Eq. (1)) and secondly the H_2 oxidation (Eq. (2)). If 1 mol of CO reacts with 0.5 mol of O_2 then the excess O_2 will start reacting with H_2 forming H_2O, therefore increasing the selectivity toward H_2O (Fig 11E) and the H_2 conversion would also increase accordingly (Fig 11C). Wootsch *et al.* and Kotobuki *et al.* reported similar trends for supported Pt catalysts [4,10].

3.2.2.3. Selectivity toward CO_2 at iso-conversion. Fig. 12 shows the 1.5% iso-conversion data of the catalysts using a C:O_2 ratio of 1:0.5 at 150 °C. With regards to the selectivity to CO_2 at low CO conversions, the Pt–Al catalyst is more selective than both the Ni containing catalysts. From the results obtained from the complete study of the PROX reactions of the catalysts, it is clear that within the PROX reaction temperature range, the Pt–Ni–Al catalyst showed better activity toward CO conversion and selectivity toward CO_2 compared to both the monometallic catalysts. Studies reported by Jo *et al.* [8] showed that a 5% Pt/Al_2O_3 catalyst gave maximum CO conversion at 150 °C, following various pre-treatments of the catalyst prior to testing. Their results and the results obtained in this study show that Pt/Al_2O_3 catalysts are active for the preferential oxidation reaction at this temperature. The Ni/Al_2O_3 catalyst, however, has not been reported in literature for this reaction, but reports have been made of Ni/Al_2O_3 catalysts being active for other oxidation reactions at much higher temperatures which are beyond the useful PROX range [7]. However, the Ni–Al catalyst at 150 °C, irrespective of the GHSVs employed, gave a maximum CO conversion of 2.5%. An iso-conversion of 20% was investigated at 180 °C using a C:O_2 ratio of 1:0.5. The Ni–Al catalysts showed very low conversions and irrespective of the GHSVs employed, a 20% conversion could not be obtained for this catalyst at this temperature.

Fig. 13 shows the selectivities to CO_2 at iso-conversion of 20% for the Pt containing catalysts using a C:O_2 ratio of 1:0.5 at a temperature of 180 °C. Under these conditions the Pt–Ni–Al catalyst is more selective to CO_2 than the mono-metallic catalyst. Selectivity toward CO_2 for the Pt–Ni–Al catalyst also showed that the addition of Pt to the mono-metallic Ni catalyst enhanced or promoted its activity, which was substantially higher than that of the mono-metallic Pt catalyst.

The Pt–Al catalyst showed better activity compared to the Ni–Al catalyst for the PROX reaction. Ni–Al has a very low affinity for CO adsorption below 200 °C, and presumably the Ni sites are still in the NiO phases making it difficult for adsorption of the reactants. The Pt containing catalysts on the other hand exhibit activity from 100 °C onwards. At temperatures below 100 °C, CO adsorbs very strongly on Pt and prevents O_2 dissociation. Elevating temperatures may cause the CO coverage and the bonding strength to be lowered resulting in free sites for O_2 dissociative adsorption [10], therefore increasing activity. The reactants CO and H_2 adsorb on Pt and the dissociated O_2 will react with either. The selectivity toward CO_2 would depend on the C:O_2 ratio. Also taking into account that the heat of CO adsorption on Pt is ~17 KJ/mol greater than the H_2 value [4], once all of the CO has been converted in the feed containing excess O_2, the selectivity toward CO_2 would decrease. This study clearly shows that the Pt–Ni–Al catalyst, which exhibited a lower onset reduction temperature in the TPR than the monometallic catalysts, showed better activity and selectivity toward CO_2 in the PROX reaction. Therefore the Pt–Ni–Al catalyst under these PROX conditions favors the oxidation of CO rather than the undesired oxi-

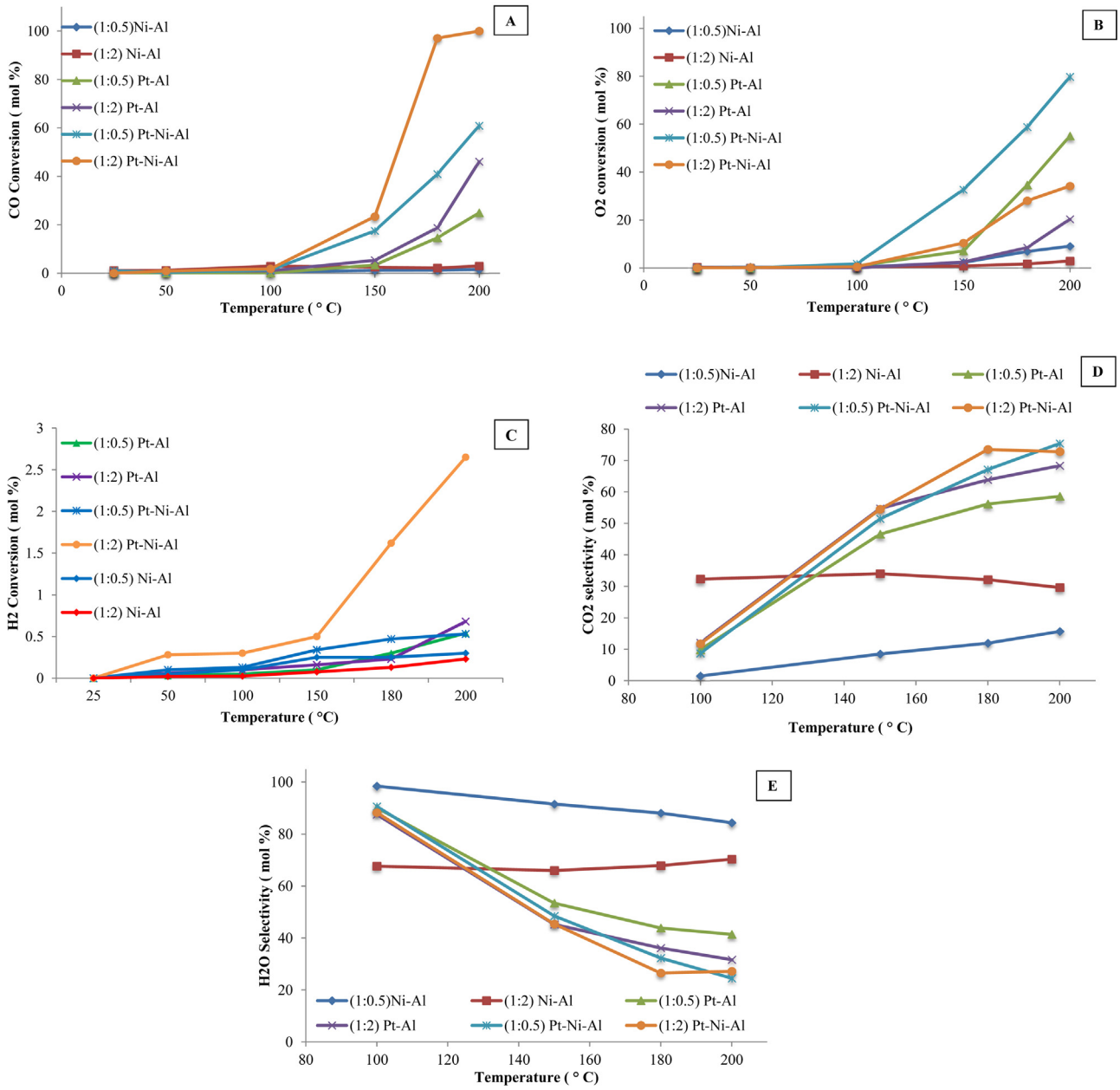

Fig. 11. PROX reactions over the catalysts with C:O_2 ratios of 1:0.5 and 1:2 using a GHSV of 12,000 h^{-1}. CO conversion (A), O_2 conversion (B), H_2 conversion (C), CO_2 Selectivity (D) and H_2O Selectivity (E).

dation of H_2 at higher PROX temperatures, which is also supported by the O_2 and H_2 conversion data.

3.3. Used catalyst characterization and mechanistic considerations

From Table 4, it can be observed that there is a decrease in the surface areas, pore volumes and pore diameters of the used catalysts compared to those of the fresh catalysts shown in Table 2. XRD patterns of the used catalysts (Supplementary information, Fig. S10) show no new phases. However, these catalysts showed signs of reduction at higher temperatures in the reactor, where the O_2 balances decreased (90–95%), but C and H balances remained constant (98–102%). Also, this could be due to the reduction–oxidation cycles that accompany the catalytic activity of the catalysts during the reactions [46]. The Mars and van Krevelan mechanism also proposes that the reactant, in this case CO, extracts lattice oxygen

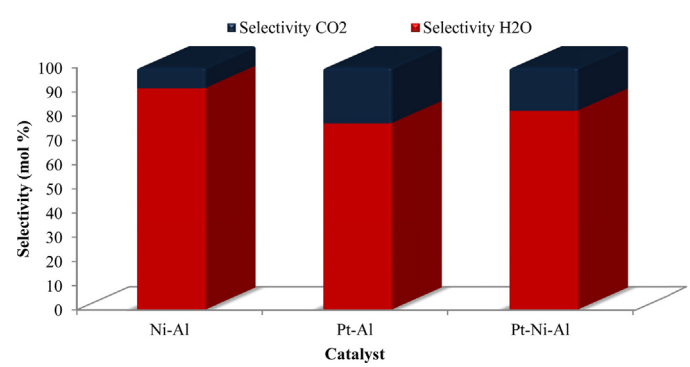

Fig. 12. Selectivity of the products at an iso-conversion of 1.5% (150 °C).

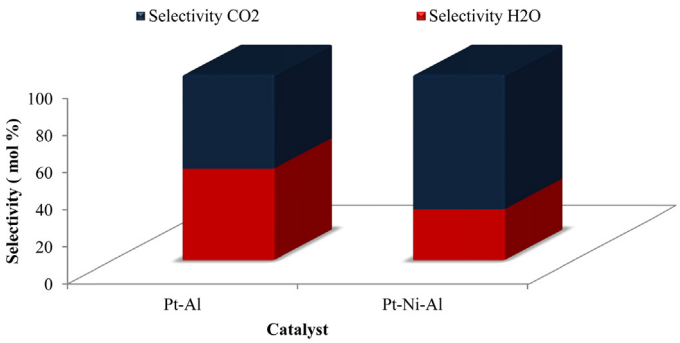

Fig. 13. Selectivity of the products at an iso-conversion of 20% (180 °C).

Table 5
XPS data of the prepared catalysts.

Sample	Binding energy (eV)			Wt (%)	
	Ni	Pt	O	Ni	Pt
Ni–Al	853.7 ($2p_{3/2}$) 859.7 ($2p_{3/2}$) 871.5($2p_{1/2}$) 877.9($2p_{1/2}$)	–	529.3 (1s)	23.1	–
Pt–Al	–	72.7 ($4f_{7/2}$) 76.0 ($4f_{5/2}$)	529.8 (1s)	–	0.41
Pt–Ni–Al	853.4 ($2p_{3/2}$) 859.2($2p_{3/2}$) 871.6($2p_{1/2}$) 877.7($2p_{1/2}$)	72.7($4f_{7/2}$) 75.8 ($4f_{5/2}$)	529.4 (1s)	23.4	0.37

from the surface layer of the catalysts, thereby reducing them [47]. This is also evident from the initial oxidation state of Ni (2+) from XPS (Table 5) and *in situ* XRD (Fig. 6) which shows formation of Ni^0. The lattice oxygen is then replenished by O_2 from the feed during the re-oxidation process [47], which is also related to the redox behavior depicted in Fig. 6. This result is evident for the supported Pt–Ni catalysts, since calcination with air, following the PROX reaction, allows the catalyst to be re-oxidized. As is evident from the XRD patterns of the used catalysts, the phases present are the metal oxide phases. The Langmuir Hinshelwood mechanism is likely also coupled with this reaction where CO and O_2 adsorb on the same adsorption sites [4,10].

4. Conclusion

XRD patterns of the fresh Ni containing samples showed that NiO species were formed on the surface of the support, whereas the PtO phases for the Pt containing catalysts could not be detected. *In situ* reduction and oxidation studies indicated that the catalysts have reversible phase changes and were stable during these phase transformations. XPS studies show that Ni and Pt are in the NiO and PtO phases. TPR and *in situ* XRD profiles indicated that the addition of Pt on the Ni containing material promoted reduction at lower temperatures, suggesting that the Pt alloys with Ni particles present on the surface of the support. The alloyed catalyst (Pt–Ni–Al) showed a lower temperature reduction and a higher degree of reducibility compared to the mono-metallic catalysts. *In situ* XRD showed that re-oxidation of this catalyst takes place at a much lower temperature compared to the mono-metallic catalysts which correlates closely to the activity of this catalyst. FTIR-CO results showed that the amount of CO adsorbed on the PtkNi–Al catalyst was higher. Importantly, the Pt–Ni–Al catalyst showed a superior CO conversion to the mono-metallic catalysts, with high selectivities toward CO_2, reducing the CO content in the feed to the target level of <10 ppm. H_2 conversions of the catalysts using stoichiometric amounts of O_2 to CO did not exceed 1%. Also using excess O_2, H_2 oxidation was minimal. Furthermore, no deactivation of the catalysts was observed. Thus, Ni catalysts with a low Pt content may be effective catalysts for the PROX of CO in H_2 rich streams.

Acknowledgements

We thank HySA for financial support, the MMU (UKZN) for the microscopic analyses, Dr. Dave Morgan, Cardiff Catalysis Institute, for XPS studies, Dr Pheladi Mohlala and Dr Marietjie duToit at SASOL R&D for FTIR-CO analyses.

Appendix A. Supplementary data

Supplementary data associated with this article can be found, in the online version, at http://dx.doi.org/10.1016/j.apcatb.2015.07.012

References

[1] G. Marbán, T. Valdés-Solís, Int. J. Hydrog. Energy 32 (2007) 1625–1637.
[2] R.K. Ahluwalia, Q. Zhang, D.J. Chmielewski, K.C. Lauzze, M.A. Inbody, Catal. Today 99 (2005) 271–283.
[3] R. Padilla, M. Benito, L. Rodríguez, A. Serrano-Lotina, L. Daza, J. Power Sources 192 (2009) 114–119.
[4] A. Wootsch, C. Descorme, D. Duprez, J. Catal. 225 (2004) 259–266.
[5] F. Mariño, C. Descorme, D. Duprez, Appl. Catal. B: Environ. 54 (2004) 59–66.
[6] L.-Y. Sung, B.-J. Hwang, K.-L. Hsueh, F.-H. Tsau, J. Power Sources 195 (2010) 1630–1639.
[7] J.A.C. Dias, J.M. Assaf, J. Power Sources 130 (2004) 106–110.
[8] M.-C. Jo, G.-H. Kwon, W. Li, A.M. Lane, J. Ind. Eng. Chem. 15 (2009) 336–341.
[9] M.M. Yung, Z. Zhao, M.P. Woods, U.S. Ozkan, J. Mol. Catal. A: Chem. 279 (2008) 1–9.
[10] M. Kotobuki, A. Watanabe, H. Uchida, H. Yamashita, M. Watanabe, J. Catal. 236 (2005) 262–269.
[11] V. Recupero, L. Pino, M. Cordaro, A. Vita, F. Cipiti, M. Laganà, Fuel Process. Technol. 85 (2004) 1445–1452.
[12] G. Kolb, Fuel Processing, Wiley, 2008.
[13] P. Sangeetha, B. Zhao, Y.-W. Chen, Ind. Eng. Chem. Res. 49 (2010) 2096–2102.
[14] S.H. Oh, R.M. Sinkevitch, J. Catal. 142 (1993) 254–262.
[15] O. Pozdnyakova, D. Teschner, A. Wootsch, J. Kröhnert, B. Steinhauer, H. Sauer, L. Toth, F.C. Jentoft, A. Knop-Gericke, Z. Paál, R. Schlögl, J. Catal. 237 (2006) 1–16.
[16] F. Cipitì, V. Recupero, Chem. Eng. J. 146 (2009) 128–135.
[17] E. Moretti, L. Storaro, A. Talon, P. Patrono, F. Pinzari, T. Montanari, G. Ramis, M. Lenarda, Appl. Catal. A: Gen. 344 (2008) 165–174.
[18] E.O. Jardim, S. Rico-Francés, F. Coloma, J.A. Anderson, J. Silvestre-Albero, A. Sepúlveda-Escribano, J. Colloid Interface Sci. 443 (2015) 45–55.
[19] M. Moreno, G.T. Baronetti, M.A. Laborde, F.J. Mariño, Int. J. Hydrog. Energy 33 (2008) 3538–3542.
[20] E.-Y. Ko, E.D. Park, K.W. Seo, H.C. Lee, D. Lee, S. Kim, Catal. Today 116 (2006) 377–383.
[21] V.P. de Souza, D. Costa, D. dos Santos, A.G. Sato, J.M.C. Bueno, Int. J. Hydrog. Energy 37 (2012) 9985–9993.
[22] Y. Kobayashi, J. Horiguchi, S. Kobayashi, Y. Yamazaki, K. Omata, D. Nagao, M. Konno, M. Yamada, Appl. Catal. A: Gen. 395 (2011) 129–137.
[23] K. Opoku-Gyamfi, A.A. Adesina, Appl. Catal. A: Gen. 180 (1999) 113–122.
[24] V.D.B.C. Dasireddy, H.B. Friedrich, S. Singh, Appl. Catal. A: Gen. 467 (2013) 142–153.
[25] P. Salagre, J.L.G. Fierro, F. Medina, J.E. Sueiras, J. Mol. Catal, A: Chem. 106 (1996) 125–134.
[26] S.M. Morris, P.F. Fulvio, M. Jaroniec, J. Am. Chem. Soc. 130 (2008) 15210–15216.
[27] S. Ren, J. Qiu, C. Wang, B. Xu, Y. Fan, Y. Chen, Chin. J. Catal. 28 (2007) 651–656.
[28] C. Li, Y.-W. Chen, Thermochim. Acta 256 (1995) 457–465.
[29] E.-Y. Ko, E. Park, K. Seo, H. Lee, D. Lee, S. Kim, Catal. Lett. 110 (2006) 275–279.
[30] B. Li, S. Kado, Y. Mukainakano, T. Miyazawa, T. Miyao, S. Naito, K. Okumura, K. Kunimori, K. Tomishige, J. Catal. 245 (2007) 144–155.
[31] H. Liu, L. Ma, S. Shao, Z. Li, A. Wang, Y. Huang, T. Zhang, Chin. J. Catal. 28 (2007) 1077–1082.
[32] J.-A. Dalmon, M. Primet, G.-A. Martin, B. Imelik, Surf. Sci. 50 (1975) 95–108.
[33] B. Pawelec, S. Damyanova, K. Arishtirova, J.L.G. Fierro, L. Petrov, Appl. Catal. A: Gen. 323 (2007) 188–201.
[34] B. Qiao, A. Wang, X. Yang, L.F. Allard, Z. Jiang, Y. Cui, J. Liu, J. Li, T. Zhang, Nat. Chem. 3 (2011) 634–641.
[35] U. Heiz, A. Sanchez, S. Abbet, W.D. Schneider, J. Am. Chem. Soc. 121 (1999) 3214–3217.
[36] G.K. Wertheim, S. Hüfner, Phys. Rev. Lett. 28 (1972) 1028–1031.
[37] B.V. Crist, Handbook of Monochromatic XPS Spectra: The Elements and Native Oxides, Wiley, 2000.

[38] Y.P.G. Chua, G.T.K.K. Gunasooriya, M. Saeys, E.G. Seebauer, J. Catal. 311 (2014) 306–313.
[39] J.C. Muijsers, J.W. Niemantsverdriet, I.C.M. Wehman-Ooyevaar, D.M. Grove, G. Van Koten, Inorg. Chem. 31 (1992) 2655–2658.
[40] E. Heracleous, A.F. Lee, K. Wilson, A.A. Lemonidou, J. Catal. 231 (2005) 159–171.
[41] E. Kiss, G. Bošković, M. Lazić, G. Lomić, R. Marinković-Nedučin, Scanning 28 (2006) 236–241.
[42] A.V. Ghule, K. Ghule, T. Punde, J.-Y. Liu, S.-H. Tzing, J.-Y. Chang, H. Chang, Y.-C. Ling, Mater. Chem. Phys. 119 (2010) 86–92.
[43] Z.-m. Liu, X.-h. Li, Z.-j. Chen, P. Ying, Z.-c. Feng, C. Li, J. Fuel. Chem. Technol. 37 (2009) 205–211.
[44] S. Wang, G.Q. Lu, App. Catal. A: Gen. 169 (1998) 271–280.
[45] H. Uchida, K. Izumi, K. Aoki, M. Watanabe, Phys. Chem. Chem. Phys. 11 (2009) 1771–1779.
[46] E. Elkhalifa, H. Friedrich, Catal. Lett. 141 (2011) 554–564.
[47] B.K. Hodnett, Heterogeneous catalytic oxidation: fundamental and technological aspects of the selective and total oxidation of organic compounds, John Wiley, 2000.